Article

Computational Studies of the Excitonic and Optical Properties of Armchair SWCNT and SWBNNT for Optoelectronics Applications

Yahaya Saadu Itas [1] , Abdussalam Balarabe Suleiman [2], Chifu E. Ndikilar [2] , Abdullahi Lawal [3], Razif Razali [4] , Ismail Ibrahim Idowu [2], Mayeen Uddin Khandaker [5,6,*] , Pervaiz Ahmad [7], Nissren Tamam [8] , Abdelmoneim Sulieman [9] and Mohammad Rashed Iqbal Faruque [10]

[1] Department of Physics, Bauchi State University Gadau, PMB 65, Gadau 751105, Nigeria; yitas@basug.edu.ng
[2] Department of Physics, Federal University Dutse, Dutse 720101, Nigeria; salam@fud.edu.ng (A.B.S.); ebenechifu@yahoo.com (C.E.N.); idowu.i@fud.edu.ng (I.I.I.)
[3] Department of Physics, Federal College of Education, Zaria 810282, Nigeria; labdullahi2@live.utm.my
[4] Department of Physics, Faculty of Science, Universiti Teknologi Malaysia, Skudai 81310, Malaysia; razifrazali@utm.my
[5] Centre for Applied Physics and Radiation Technologies, School of Engineering and Technology, Sunway University, Bandar Sunway 47500, Malaysia
[6] Department of General Educational Development, Faculty of Science and Information Technology, Daffodil International University, DIU Rd, Dhaka 1341, Bangladesh
[7] Department of Physics, University of Azad Jammu and Kashmir, Muzaffarabad 13100, Pakistan; pervaiz_pas@yahoo.com
[8] Department of Physics, College of Sciences, Princess Nourah Bint Abdulrahman University, P.O. Box 84428, Riyadh 11671, Saudi Arabia; nmtamam@pnu.edu.sa
[9] Department of Radiology and Medical Imaging, College of Applied Medical Sciences, Prince Sattam Bin Abdulaziz University, P.O. Box 422, Alkharj 11942, Saudi Arabia; a.sulieman@psau.edu.sa
[10] Space Science Centre (ANGKASA), Institute of Climate Change (IPI), Universiti Kebangsaan Malaysia, Bangi 43600, Malaysia; rashed@ukm.edu.my
* Correspondence: mayeenk@sunway.edu.my

Abstract: In this study, the optical refractive constants of the (5, 5) SWBNNT and (5, 5) SWCNT systems were calculated in both parallel and perpendicular directions of the tube axis by using Quantum ESPRESSO and YAMBO code. It also extended the optical behaviors of (5, 5) SWCNT and (5, 5) SWBNNT to both perpendicular and parallel directions instead of the parallel directions reported in the literature. It also looked at the effects of the diameter of the nanotube on the optical properties instead of chiral angles. From our results, the best optical reflection was found for (5, 5) SWBNNT, while the best optical refraction was found with (5, 5) SWCNT. It was observed that the SWCNT demonstrates refraction in both parallel and perpendicular directions, while (5, 5) SWBNNT shows perfect absorption in perpendicular direction. These new features that appeared for both nanotubes in perpendicular directions were due to new optical band gaps, which appear in the perpendicular directions to both nanotubes' axis. The electron energy loss (EEL) spectrum of SWBNNT revealed the prominent π- and π + δ- Plasmon peaks, which demonstrates themselves in the reflectivity spectrum. Furthermore, little effect of diameter was observed for the perpendicular direction to both nanotubes' axis; as such, the combined properties of (5, 5) SWBNNT and (5, 5) SWCNT materials/systems for transmitting light offer great potential for applications in mobile phone touch screens and mobile network antennas. In addition, the studies of optical properties in the perpendicular axis will help bring ultra-small nanotubes such as SWCNT and SWBNNT to the applications of next-generation nanotechnology.

Keywords: excitonic properties; SWCNT; SWBNNT; optical band gap; optical refraction; optical extinction

1. Introduction

Carbon nanotubes are tubular sheets of nanomaterials formed by rolling graphene sheets into a tubular form, and they were introduced to the field of nanoscience and nanotechnology in 1991 [1,2]. They exist in different geometries, depending on the chirality and diameter; these are armchair, zigzag, and chiral nanotubes [3]. For example, rolling the graphene sheet from its corner gives a different shape than when it is rolled from its edge. As such, the structure of materials in the form of nanotubes is determined by the chiral indices "n" and "m", which represent the coordinates of the rolling of the graphene sheet. In any case, the calculation of the chirality is based on the following Equation (1) [3]:

$$C = na_1 + ma_2 \tag{1}$$

where a_1 and a_2 are the chiral vectors of the graphene sheet. The nanotubes are called armchairs when n = m, for example (3, 3), (4, 4), (5, 5), (6, 6), and so on. It is called zigzag when 'n' is not equal to 'm', for example (5, 4), (8, 3), and so on. However, the nanotubes are called chiral when 'm' = 0. In our case, we were dealing with the armchair form of both SWCNT and SWBNNT with (5, 5) configurations. The armchair nanotubes show electrical properties similar to metals, while the zigzag and chiral nanotubes possess electrical properties similar to semiconductors. Boron nitride nanotubes are also obtained in a similar way by rolling a sheet of hexagonal boron nitride, and their chirality is also calculated based on the aforementioned Equation (1).

Since 1991, two types of carbon nanotubes have been discovered [4]. Single-walled carbon nanotubes (SWCNTs) and multi-walled carbon nanotubes (MWCNTs) have consistently been used in nanotechnology applications because of their novel thermal, mechanical, electrical, optical, and magnetic properties [5]. The size and chirality of the CNT depend on the diameter and length of the nanotubes. In today's nanoscience and technology, SWCNTs have been found to be used as sensors, LED devices, and photovoltaic and thermal reservoirs [6]. A review of the literature revealed some studies on the large armchair of SWCNTs such as (7, 7), (8, 8), (10, 10), and (12, 12) SWCNTs. Some research was also conducted on the ultra-small SWCNTs, such as (3, 3) and (4, 4) SWCNTs. However, only a few works of the literature showed the existence of (5, 5) SWCNT studies. This work was designed to solve some crucial issues regarding (5, 5) SWCNT, especially the optical properties.

On the other hand, boron nitride nanotubes (BNNTs) are rolled sheets of hexagonal boron nitride and have similar physical geometries to CNTs. They also exist in an armchair, zigzag, and chiral form [7]. They are therefore regarded as having close structural analogs of carbon nanotubes [8], because carbon atoms are alternatively replaced with boron and nitrogen atoms in a hexagonal lattice. BNNTs are perfect insulators on all configurations with a wide bandgap of 5.5 eV [9]. BNNTs show remarkable resistance to oxidation and greater thermal stability; such remarkable features make them excellent candidates in mechanical reinforcement, radiation shielding, transparent bulk composites, etc. [10]. However, both CNTs and BNNTs have some common properties [7], such as high strength, high stiffness, high thermal conductivity, low density, and high length to diameter [7].

By considering the common features found in CNTs and BNNTs, scientists have thought of combining these two novel materials in order to come up with bridged applications that can be put into next-generation technology and applications. For example, experimental studies were conducted on the synthesis of thermally stable CNT and BNNT hetero materials [11], and the results showed promising applications of CNT and BNNT in light emitting diodes (LED). Similarly, another computational approach was performed for the electronic properties of (5, 5) SWCBNNT nanostructures, which predict the excellent ability of these materials to serve as gas sensors [12]. Further review of the literature showed that many experimental and theoretical studies have been conducted on the optical properties of nanomaterials in parallel directions only (see Table 1). Besides this, very few quantum simulation studies are available on ultra-small nanotubes such as (5, 5) CBNNT

systems. In order to bridge this gap, this work performed a detailed simulation on the effects of excitons across parallel and perpendicular directions to both nanotubes' axis, and such a comparative study was performed here for the first time. It also focused on the potential of two nanomaterials for comparative analysis of the optical properties of (5, 5) SWCNT and (5, 5) SWBNNT and provided some possible explanations for their use in optoelectronics. This work also explored the effects of the diameter of the nanotubes on the excitons, instead of the chiral angle, as studied by many works available in the literature (Table 1).

Table 1. Reported studies on the optical properties of nanomaterials.

S/No.	Research/Experiment	Results Obtained	Ref.
1	Optical properties of carbon nanotubes	The studies of the excitonic properties were implemented in the parallel direction to the nanotube axis. The result predicted that dark excitons affect the potential of carbon nanotubes for applications as radiation shields.	[13]
2	Optical properties of CNT single-band tight-binding approximation	The studies were applied in the parallel direction to the tube axis, and results revealed optical transitions between Van Hove singularities. The authors recommend further investigations in the perpendicular direction to the tube axis.	[14]
3	Theoretical studies on optical properties of individual carbon nanotubes	It reported that experimental and simulation studies shall be carried out on the ultra-small carbon nanotubes in all directions to confirm theoretical predictions.	[15]
4	Theoretical investigation of the optical properties of boron nitride nanotubes	The optical properties are affected by the polarization directions (parallel) as well as the radius of the nanotube.	[16]
5	Theoretical studies on vibrational and optical properties of BNNTs	Studied Raman spectroscopy and EELS of BNNTs in the parallel direction to the tube axis. It recommends that more studies need to be carried out in the perpendicular directions to bring BNNTs into the optoelectronics world.	[17]
6	Quantum simulation using quantum ESPRESSO and YAMBO codes	Studied the excitonic properties and effects of diameter on the polarization of SWCNTs and SWBNNTs in both the parallel and perpendicular directions.	This work

2. Methodology

In this research, Kohn-Sham equations were applied by implementing the DFT *ab initio* framework within the Perdiew-Burke-Emzahope (PBE) exchange functional. The energy cut-off value for the construction of the plane-wave basis set for both SWCNT and SWBNNT was achieved at 50 Ry, and the k-point value, which correlates to the ecut value, was $1 \times 1 \times 28$ k-mesh. This gave a total of 28 nk-points in the first Brillouin zone (BZ). The norm-conserving pseudopotentials were used to calculate the ion-electron's attractive interactions. Furthermore, GW-BSE calculations were performed with YAMBO code, and these were used to calculate the quasi-particle energies and optical properties of the (5, 5) SWCNT and (5, 5) SWBNNT systems. A plane-wave basis set was arranged, such that the total energy convergence was 5.5×10^{-6} Ry per carbon atom. In order to avoid inter-tube interactions, we created a vacuum from the optimized lattice parameters concerning the total energy, and the calculations were performed using a non-spin polarized DFT to save computational cost. To ensure accurate results in this study, the nanotube was appropriately relaxed to appropriate geometries. In the SWCNT, the tube length and the tube height were chosen as 5.03 Å and 3.26 Å, respectively. The chiral/translation vectors were constructed such that n = 5 and m = 5 to ensure the proper armchair chirality. The maximum force, stress, and displacements were set at 0.06 eV/Å, 0.06 GPa and 6×10^{-4} Å, respectively. The unit cell volume was 5515.67 Å^3 with lattice parameters a = 16.68 Å and c = 7.68 Å.

3. Results and Discussion

3.1. Band Gap

Computational condensed matter physics used DFT simulations to obtain the electronic and optical properties of both the bulk and nano-forms of materials with all configurations. It explained the correlated relationship between the optical bandgap and electronic bandgap of materials, as can be viewed in the ultraviolet region of the EM spectrum. As presented in Figure 1a, highly non-metallic properties can be observed from (5, 5) SWBNNT, which demonstrates a bandgap of 5.4 eV (Figure 1b); this value falls within the range of the bandgap obtained for BNNTs [18] as reported in ref. [19]. There are also more energy states in the conduction band than in the valence band for the (5, 5) SWBNNT system. The electronic bands and density of the states were also calculated for the (5, 5) SWCNT system, and zero bandgap can be seen with bands crossing the Fermi level and intersecting at the Dirac point as presented in Figure 2a. A justification is that the (5, 5) SWCNT system is metallic, as are other armchair CNTs [20]. In contrast to BNNTs, more energy states appear in the valence band than in the conduction band (Figure 2b), and the density of the state revealed three different sub-bands forming both inter-band and intra-band optical transitions (Figure 2b). There is therefore strong optical absorption as the energy of the incident photon equalizes the corresponding sub-bands [21]. In each case, there is a specific sub-band that has been identified by one integer that denotes the size of the sub-band. Three optical band gaps that are parallel to the direction of the tube axis are seen. Optical absorption occurs when the difference in sub-band energies equals the energy of the incident photon. There is a strong correlation between the chirality of the (5, 5) SWCNT and its optical transitions. This is because as the diameter of the (5, 5) SWCNT increases, there occurs a shift in the absorption peaks to greater photon energies [22].
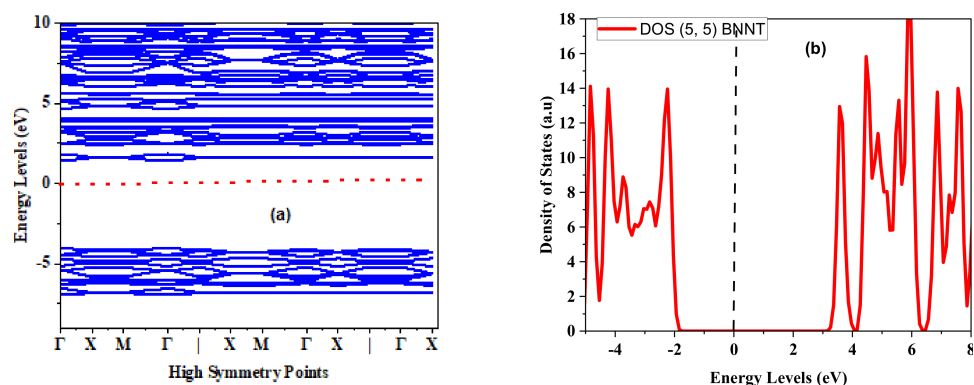

Figure 1. (**a**) The electronic bands and (**b**) density of the states of (5, 5) SWBNNTs.
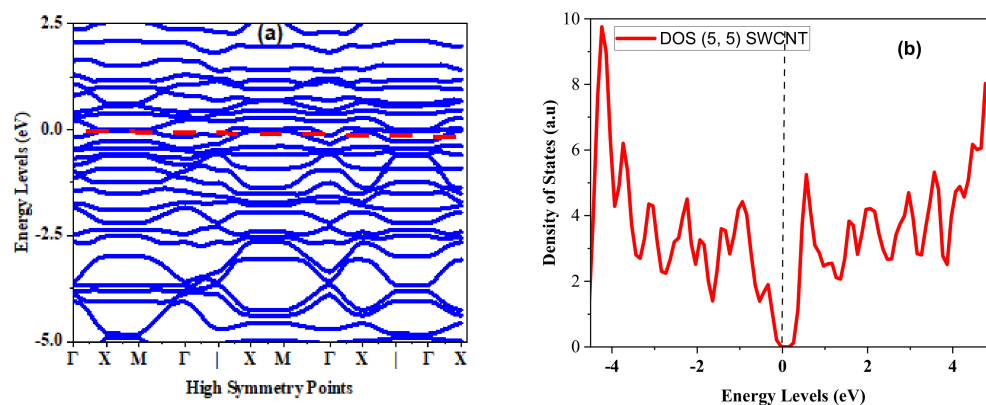

Figure 2. (**a**) The electronic bands and (**b**) density of the states of (5, 5) SWCNTs.

3.2. Dielectric Constant

Simulation analyses were conducted on the dielectric function of the real and imaginary parts of the (5, 5) SWBNNT and SWCNT in both the lower range and higher range. The studies applied to both the parallel and perpendicular directions of the nanotube axis of the two systems under study, as presented in Figure 3.

The linear response function of the (5, 5) SWBNNT and SWCNT structures to electromagnetic radiation can be explained in terms of the dielectric function [23]:

$$\varepsilon(\omega) = \varepsilon_1(\omega) + i\varepsilon_2(\omega) \tag{2}$$

where ε, is the frequency of the incident, $\varepsilon_1(\omega)$ is the frequency of the incident light for the real part, and $i\varepsilon_2(\omega)$ is the dielectric function in the imaginary part. The contribution of s and p orbitals was so affected by polarization [24], except for those orbitals close to the Fermi energy level.

$$n = \sqrt{\varepsilon_1} \tag{3}$$

The peaks of the imaginary parts of the dielectric constants of both SWCNTs and SWBNNTs illustrate the optical band gaps. In this work, the results of the optical refractive constants of the (5, 5) SWBNNT and (5, 5) SWCNT systems were found in both parallel and perpendicular directions. It was calculated that 1.3 and 1.5 eV were obtained for (5, 5) SWBNNT, and the values of 1.35 and 1.09 were obtained, respectively, for parallel and perpendicular to the tube axis for (5, 5) SWCNT. The optical gap was also larger for (5, 5) SWBNNT than (5, 5) SWCNT, which justifies that SWBNNT is a wide gap material and SWCNT is a zero-gap material. It was also observed that the nanotube diameter affected the real dielectric constant and the refractive index [25]. As such, increasing the diameter of the nanotube decreased the real dielectric constant. In condensed matter physics involving a non-spinning polarized case, we calculated the imaginary part of the dielectric function from the expression:

$$i\varepsilon_{\alpha\beta}(\omega) = \frac{\hbar^2 e^2}{\pi m^2 \omega^2} \sum_c \int dk \langle C_k | P^\alpha | v_k \rangle \langle v_k | P^\beta | C_k \rangle \, X \, \delta(\varepsilon_{ck} - \varepsilon_{vk} - \omega) \tag{4}$$

where m is the rest mass of an electron, e is the amount of the charge on an electron with mass m, C_k is the empty conduction band, and v_k is the occupied valence states. For calculation of the real part of the dielectric part, we adopted the Kramers–Kronig equation:

$$r\varepsilon_{\alpha\beta}(\omega) = \delta_{\alpha\beta} + \frac{2}{\pi} P \int_0^\infty \frac{\omega' i\varepsilon_{\alpha\beta}(\omega')}{\omega'^2 - \omega^2} d\omega' \tag{5}$$

where the subscripts α and β denote the components of directions.

As presented in Figure 3a, the optical gap of the (5, 5) SWCNT in the imaginary dielectric was larger in the parallel direction than in the perpendicular direction; as such, the dielectric function of (5, 5) SWCNT was anisotropic [26,27]. Furthermore, the dielectric function for the z-direction was higher than in the x-direction in the majority of the energy ranges. The presence of peaks in the imaginary part of the dielectric function indicated the occurrence of inter-band transitions [28]. In the case of the (5, 5) SWBNNT, the optical gap was larger in the perpendicular direction than in the parallel direction; three smaller peaks can be seen in the parallel direction for (5, 5) SWBNNT, and this demonstrates that BNNTs can also be anisotropic [29].
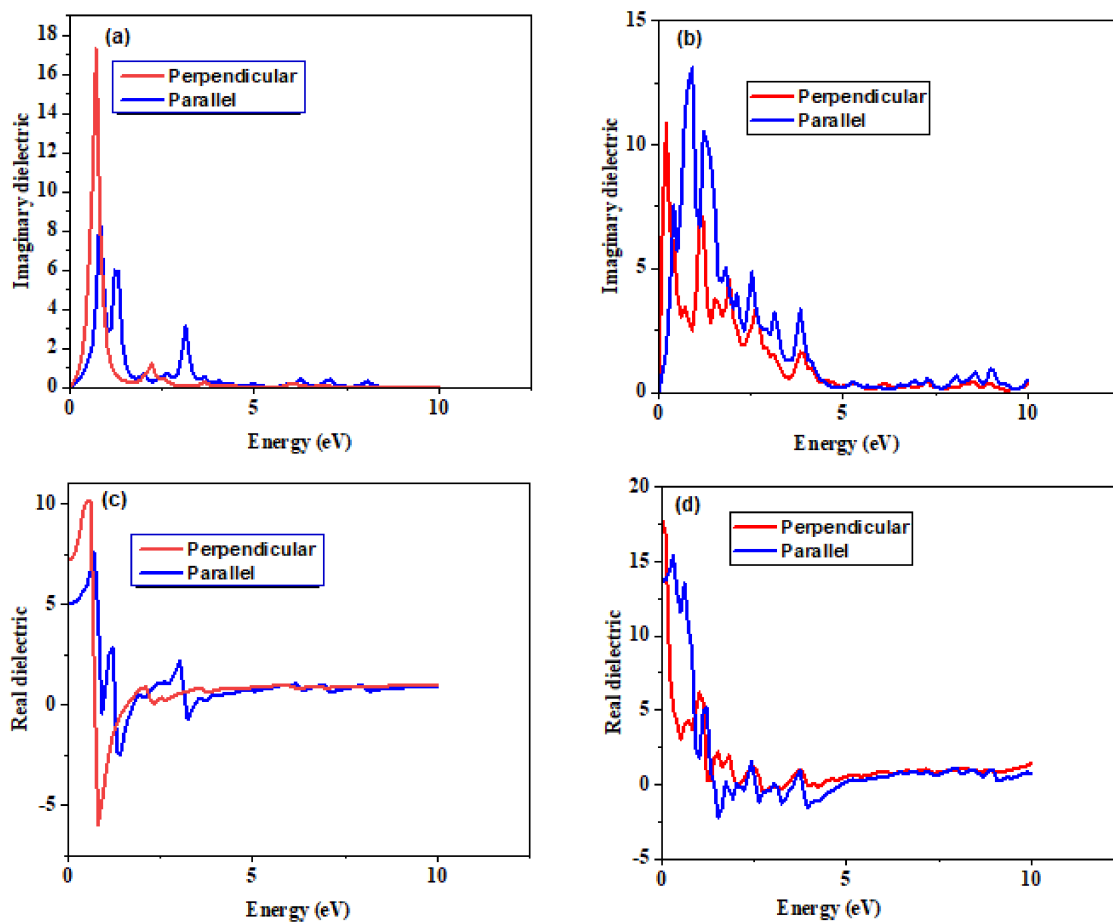
Figure 3. Dielectric functions of (5, 5) SWBNNT and SWCNT systems. (**a**) Imaginary dielectric for (5, 5) SWBNNT, (**b**) imaginary dielectric for (5, 5) SWCNT, (**c**) real dielectric for (5, 5) SWCBNNT, and (**d**) real dielectric for (5, 5) SWCNT.

3.3. Electronic Charge Distributions

The energy lost/released by an electron in traversing from one band to another was calculated for both (5, 5) SWCNT and SWBNNT systems. The calculated charge distributions of each of the two nanotubes are presented in Figure 4. In all cases, the peaks of (ω) appeared as a result of combined excitations of different photons with various frequencies. The expanded distance of the electron energy loss by the excitons in (5, 5) SWBNNT (Figure 4a) related to the absorption peak [30]. This shows that the distribution of the valence electrons has fast convergence. More energies were lost in the perpendicular direction than in the parallel direction for (5 5) SWBNNT; this can be seen by the appearance of peaks at 2.0 eV, which correspond to the energy in the plasma frequency and 2.7 eV (red) respectively. Therefore, the maximum energy was lost as a result of the effect of incident electromagnetic radiation with matter. In the (5, 5) SWCNT structure, the maximum energy loss was in the parallel direction rather than in the perpendicular direction; this can be seen from the peak at 5.0 eV presented in Figure 4b. This value is also associated with plasma energy. Furthermore, the charge distributions were more in the direction parallel to the (5, 5) SWBNNT tube axis. Sharp π-electronic peaks [31] were seen parallel and perpendicular to the tube axis, as shown in Figure 4a. Plasmon peaks were seen at 4.5 eV and 5.2 eV parallel and perpendicular to the tube axis, respectively. These results indicate that the energy loss variations had the same amplitude in (5, 5) SWCNT. The energy loss region of the EELS in Figure 4a,b is generally less than 50 eV; this is specifically called the valence electron energy loss spectroscopy (VEELS) because it is dominated by the collective excitations of the Plasmon (valence electrons) and inter-band transitions [32].
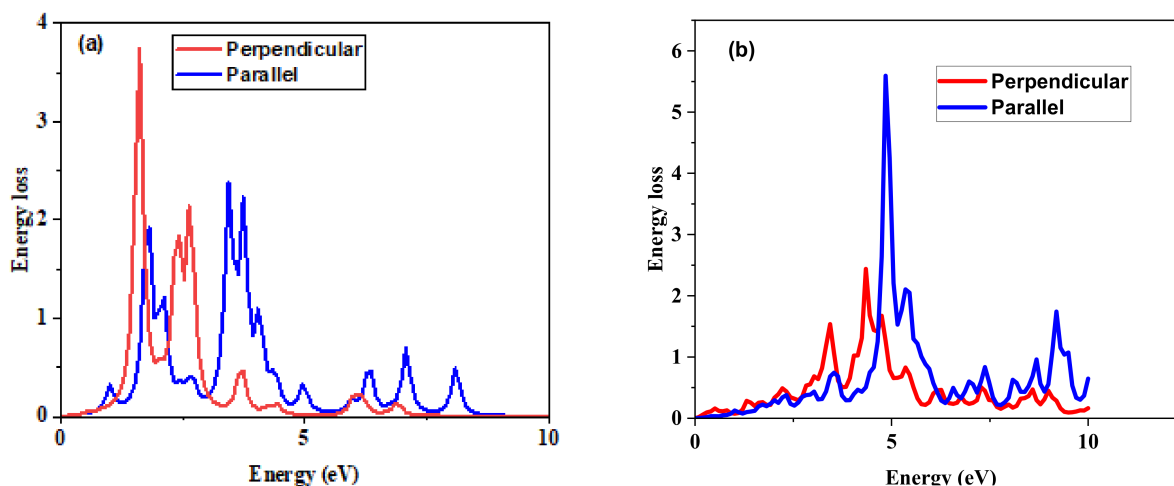
Figure 4. Electron energy loss variations of (**a**) armchair (5, 5) SWBNNT and (**b**) armchair (5, 5) SWCNT structures.

3.4. Reflection

It is very crucial to consider the volume of a monochromatic wavelength incident on a material to accurately describe its response to electromagnetic radiation. This can be achieved through studies of optical reflection and transmittance. We studied this via a spectrum of complex refractive index as a function of a single surface reflectance and phase function in both the parallel and perpendicular directions of the nanotube axis. For the (5, 5) SWBNNT structure presented in Figure 5a, the maximum reflection can be seen perpendicular to the nanotube axis, corresponding to the energy of 1.7 eV in the electromagnetic spectrum. In addition, low-intensity reflections are seen in the parallel direction of the tube axis due to π-π electronic excitations. For the (5, 5) SWCNT structure in Figure 5b, there are maximum optical reflection peaks at 0.1 eV for parallel directions and perpendicular directions. More peaks can be seen in the perpendicular direction than in the parallel direction, occurring at 5.7, 6.3, 7.7, and 9.6 eV, respectively. This illustrates that (5, 5) SWCNT has a higher optical reflection in the direction perpendicular to the nanotube axis [31].
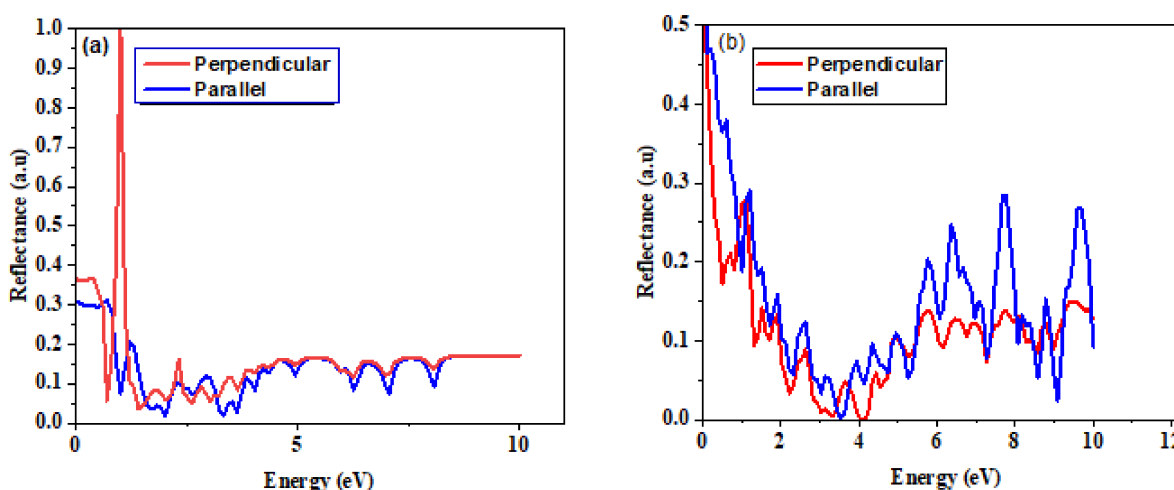

Figure 5. Optical reflection of (**a**) armchair (5, 5) SWBNNT and (**b**) armchair (5, 5) SWCNT structures.

3.5. Absorption

This study presently simulated the variation of the absorption coefficient of the (5, 5) form of SWCNT and SWBNNT structures both parallel and perpendicular to the nanotubes axis. To further reveal more about the fraction of the incident photon absorbed

or transmitted, we compared the total light reflected and the total light transmitted with the incident energy. The fraction of light absorbed per given distance in a medium was termed the absorption coefficient. In investigating the optical properties of nanomaterials with zero band gaps, it was essential to calculate the optical absorption because it is another way to understand the material's optical constants, such as refractive index. We analyzed the coefficient of absorption $\alpha(\omega)$ for the incident light with frequency ω via the well-known expression $P(\omega) = \chi(\omega)E(\omega)$, with optical susceptibility $\chi(\omega)$, where $P(\omega)$ is the macroscopic polarization and $E(\omega)$ is the electric field [33]:

$$\alpha(\omega) \sim \omega Im\chi(\omega) = Im[\frac{j(\omega)}{\omega A(\omega)}] \qquad (6)$$

where $j(\omega)$ is the macroscopic current density.

Figure 6 shows the region of low range and high range energies. The peaks in the low range energy appear because of the total intra-band excitations to the empty conduction states from the occupied valence states. The corresponding valence-to-conduction band transition can be seen from the peaks in the z-direction absorption spectra. The spectrum of SWBNNT presented in Figure 6a shows only one peak, which occurred at 0.7 eV in the perpendicular direction. This peak was a result of transitions between optical-electronic states [34]. Zero peaks can be seen in the parallel direction, which justifies zero absorption. The presence of a peak at 0.7 eV shows that SWBNNT only absorbed photons in the ultraviolet region, and there was no absorption in the visible region; therefore, (5, 5) SWBNNT was regarded as the poor absorber of photons in the visible region.
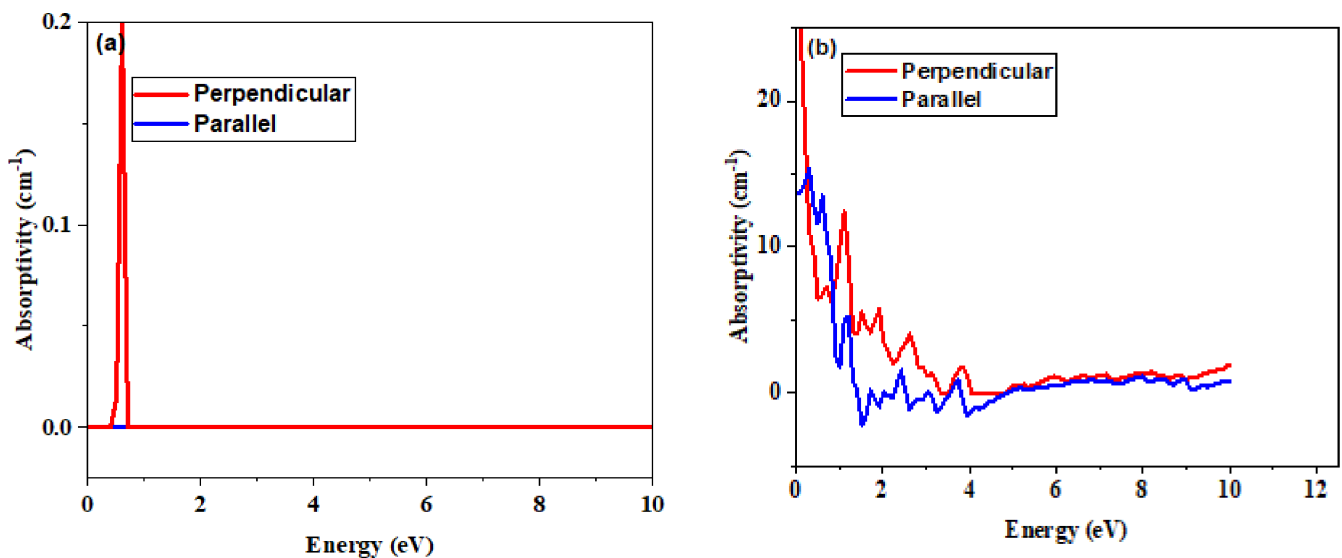

Figure 6. Optical absorptivity of (**a**) armchair (5, 5) SWBNNT and (**b**) armchair (5, 5) SWCNT structures.

In the case of (5, 5) SWCNT, peaks appeared in both parallel and perpendicular directions (Figure 6b). The peak in the parallel direction was due to the electronic transitions between sub-bands, while the peak in the perpendicular direction was due to the C-C SP^2 hybridized regions. The intensity of the peak was higher in the perpendicular direction than in the parallel direction for (5, 5) SWCNT. These two peaks demonstrate the strong absorption properties of (5, 5) SWCNT in both the UV and visible regions. To further confirm the absorption behaviors of these two nanotubes, we studied the optical properties of the (5, 5) form of both SWCNT and SWNNT via a simulation of UV-Vis [34] spectra. The results are presented in Figure 7a,b.
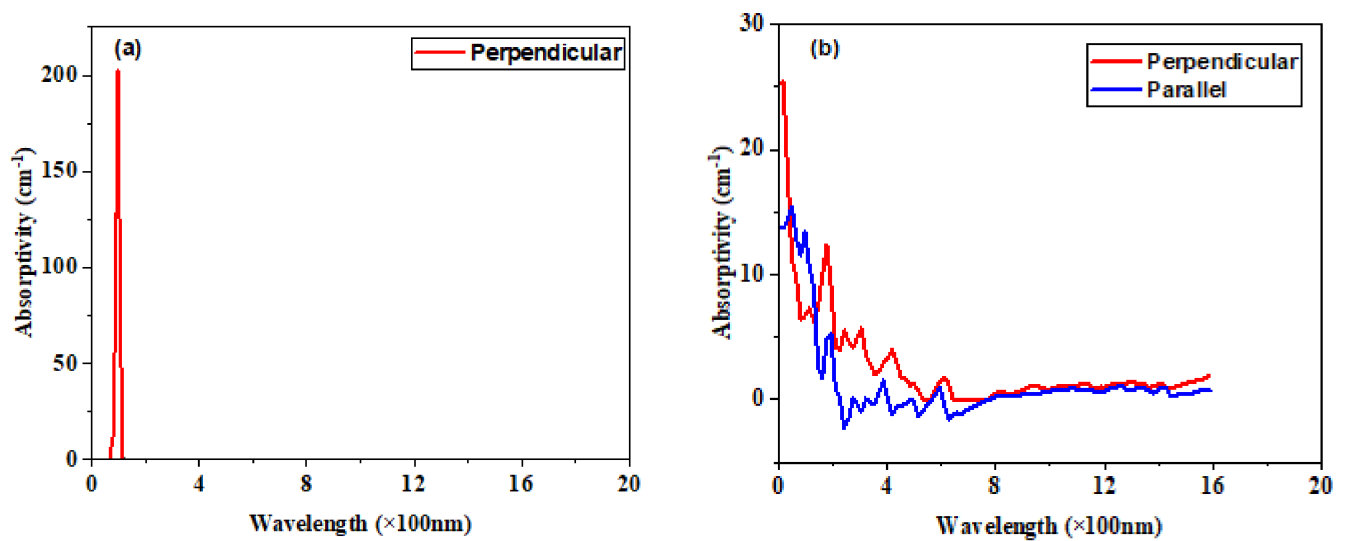
Figure 7. UV-Vis spectra of (**a**) armchair (5, 5) SWBNNT and (**b**) armchair (5, 5) SWCNT structures.

The results were calculated using Equation (7) in terms of the wavelength of monochromatic light absorbed by both systems:

$$\lambda = \frac{hC}{E} \qquad (7)$$

where *E* is the energy of the incident photon in eV

It can be seen that armchair SWBNNT showed high absorption perpendicular to the nanotube axis only. This occurred at the wavelength range of 100 nm (see Figure 7a), which corresponded to the range of wavelength in the UV region (100–400 nm) [35]. As such, armchair SWBNNT demonstrates high absorption in the ultraviolet region. Similar analyses were carried out on armchair SWCNT, as shown in Figure 7b. In this case, (5, 5) SWCNT demonstrated high absorption in all directions in the same ultraviolet region as SWBNNT. The combined absorption properties of these nanomaterials in the ultraviolet region revealed that they can be used as impurity detectors. The similarities observed in Figure 6a,b and Figure 7a,b confirmed that electromagnetic energy is a function of wavelength.

3.6. Refraction

The index of refraction was fundamentally determined by the crystal structure; it is the measure of the velocity of light of a given wavelength to its velocity in a medium:

$$R(\omega) = \frac{(n-1)^2 + k^2}{(n+1)^2 + k^2} \qquad (8)$$

where *n* is the index of refraction and k is the extinction coefficient in the real and imaginary parts, respectively, of the complex refractive index. As presented in Figure 8a, higher refractions were found parallel to the (5, 5) SWBNNT axis than the perpendicular axis; however, the extinction of refraction, which is a function of the imaginary dielectric, was higher perpendicular to the nanotube axis. Figure 8b showed that 0.1 eV was obtained for maximum optical extinction, and 2.0 eV was obtained for optical refraction, which confirms the dielectric function. Refraction was seen both parallel and perpendicular to the tube axis. The ability of (5, 5) SWCNT to refract in all directions brings it to be a potential candidate for fiber optics and magnifying lenses [35]. Our results are comparable to the results obtained for (10, 10) armchair SWCNT [36]. The coefficient of extinction is the amount of energy loss as a result of charge interactions between medium and light. We studied this to understand the number of transmissions across refracting systems, which we

achieved by taking measurements of the photon frequency transmitted through SWBNNT and SWCNT as a function of energy. Figure 9a,b reveals that there was perfect transmission in all directions, and for all the SWBNNT and SWCNT structures studied, this occurred in the energy range below 1 eV.
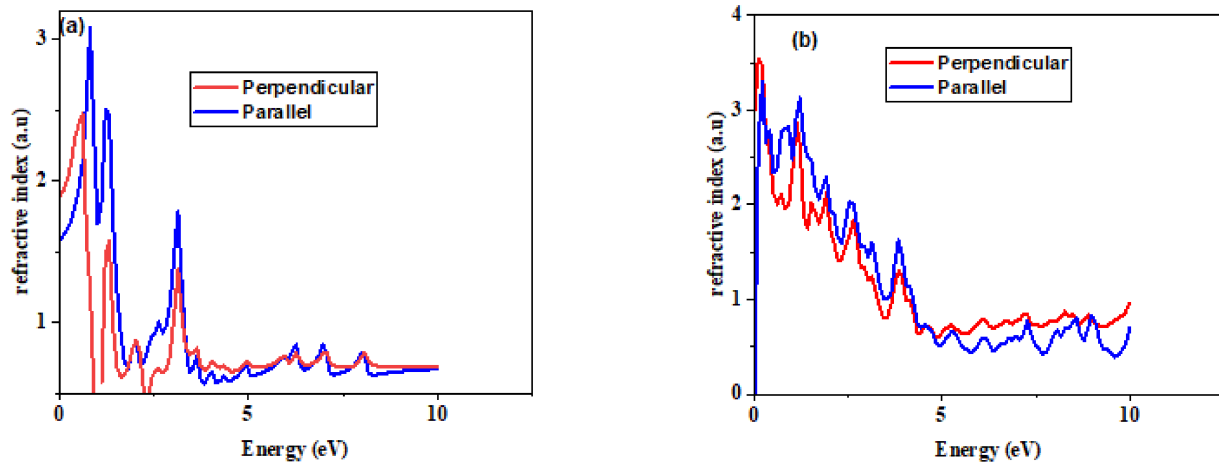

Figure 8. The optical refractive index of (**a**) armchair (5, 5) SWBNNT and (**b**) armchair (5, 5) SWCNT structures.
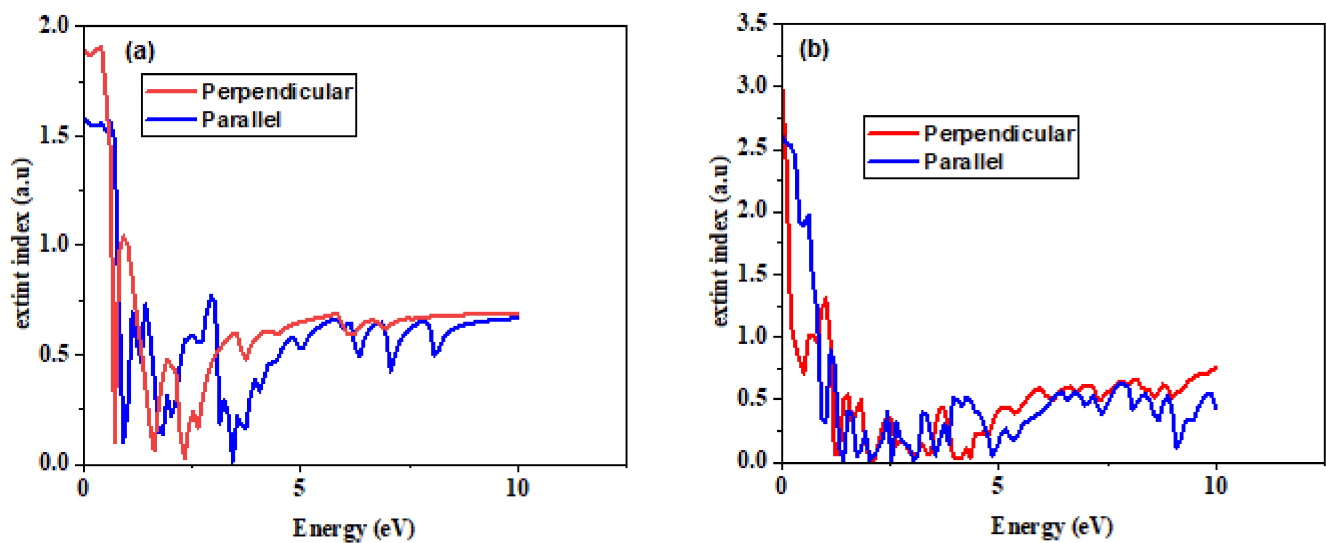

Figure 9. Optical extinction of (**a**) armchair (5, 5) SWBNNT and (**b**) armchair (5, 5) SWCNT structures.

The combined properties of (5, 5) SWBNNT and SWCNT materials to transmit light brings their applications for use in mobile phone touch screens [37] and mobile network antennas.

4. Conclusions

The excitonic properties of (5, 5) SWBNNT and (5, 5) SWCNT were studied using DFT and GW-BSE simulation methods. SWBNNT demonstrated optical bandgaps in both the parallel and perpendicular directions, while SWCNT showed a weaker optical gap in the perpendicular direction. It is generally reported that the electron energy is lost due to the valence electron energy loss spectroscopy because it is dominated by the collective excitations of the Plasmon (valence electrons) and inter-band transitions. However, in this study, the calculated charge distribution revealed that electron energy was lost due to the combined excitations of different photons with various frequencies. In addition to their various optical responses in various directions, SWBNNT showed

reflection only in the perpendicular direction, while SWCNT reflected in all directions. The (5, 5) SWBNNT absorbed phonon only in the perpendicular direction, which suggests that it cannot be used for perfect absorption applications. On the other hand, (5, 5) SWCNT showed peaks in both directions; the peak in the parallel direction was due to the electronic transitions between sub-bands, while the peak in the perpendicular direction was due to the C-C SP^2 hybridized regions. It is therefore regarded that SWCNT possesses strong absorption properties and is suitable to be used in absorption applications, such as impurity detectors. The dielectric property of (5, 5) SWCNT confirmed that 0.1 eV was obtained for maximum optical extinction and 2.0 eV was obtained for optical refraction. This showed that SWCNT transmits and refracts light, and refractions were also seen in both parallel and perpendicular directions, which brings its application to fiber optics and magnifying lenses. There was also a perfect transmission at low energy ranges for both systems. The combined properties of (5, 5) SWBNNT and SWCNT materials to transmit light make them suitable to be used in mobile phone touch screens and mobile network antennas.

References

1. Saifuddin, N.; Raziah, A.Z.; Junizah, A.R. Carbon Nanotubes: A Review on Structure and Their Interaction with Proteins. *J. Chem.* **2012**, *2013*, 1–18. [CrossRef]
2. Itas, Y.S.; Ndikilar, C.E.; Zangina, T. Carbon Nanotubes: A Review of Synthesis and Characterization Methods/Techniques. *Int. J. Sci. Technoledge* **2020**, *8*. [CrossRef]
3. Eatemadi, A.; Daraee, H.; Karimkhanloo, H.; Kouhi, M.; Zarghami, N.; Akbarzadeh, A.; Abasi, M.; Hanifehpour, Y.; Joo, S.W. Carbon nanotubes: Properties, synthesis, purification, and medical applications. *Nanoscale Res. Lett.* **2014**, *9*, 393. [CrossRef] [PubMed]
4. Pandey, P.; Dahiya, M. Carbon nanotubes: Types, methods of preparation and applications. *Int. J. Pharm. Sci. Res.* **2016**, *1*, 15–21.
5. Dresselhaus, M.S.; Dresselhaus, G.; Charlier, J.-C.; Hernandez, E.R. Electronic, thermal and mechanical properties of carbon nanotubes. *Philos. Trans. R. Soc. London. Ser. A Math. Phys. Eng. Sci.* **2004**, *362*, 2065–2098. [CrossRef]
6. Abdalla, S.; AlMarzouki, F.; Al-Ghamdi, A.A.; Abdel-Daiem, A. Different Technical Applications of Carbon Nanotubes. *Nanoscale Res. Lett.* **2015**, *10*, 1–10. [CrossRef]
7. Celik-Aktas, A.; Zuo, J.M.; Stubbins, J.F.; Tang, C.; Bando, Y. Structure and chirality distribution of multiwalled boron nitride nanotubes. *Appl. Phys. Lett.* **2005**, *86*, 133110. [CrossRef]
8. Dolati, S.; Fereidoon, A.; Kashyzadeh, K.R. A Comparison Study between Boron nitride nanotubes and Carbon nanotubes. *Int. J. Emerg. Technol. Adv. Eng.* **2012**, *2*, 1–11.
9. Saikia, N.; Pati, S.K.; Deka, R.C. First principles calculation on the structure and electronic properties of BNNTs functionalized with isoniazid drug molecule. *Appl. Nanosci.* **2012**, *2*, 389–400. [CrossRef]

10. Zhang, D.; Zhang, S.; Yapici, N.; Oakley, R.; Sharma, S.; Parashar, V.; Yap, Y.K. Emerging Applications of Boron Nitride Nanotubes in Energy Harvesting, Electronics, and Biomedicine. *ACS Omega* **2021**, *6*, 20722–20728. [CrossRef]

11. Itas, Y.S.; Ndikilar, C.E.; Zangina, T.; Hafeez, H.Y.; Safana, A.A.; Khandaker, M.U.; Ahmad, P.; Abdullahi, I.; Olawumi, B.K.; Babaji, M.A.; et al. Synthesis of Thermally Stable *h*-BN-CNT Hetero-Structures via Microwave Heating of Ethylene under Nickel, Iron, and Silver Catalysts. *Crystals* **2021**, *11*, 1097. [CrossRef]

12. Itas, Y.S.; Suleiman, A.B.; Ndikilar, C.E.; Lawal, A.; Razali, R.; Khandaker, M.U.; Ahmad, P.; Tamam, N.; Sulieman, A. The Exchange-Correlation Effects on the Electronic Bands of Hybrid Armchair Single-Walled Carbon Boron Nitride Nanostructure. *Crystals* **2022**, *12*, 394. [CrossRef]

13. Saito, R.; Dresselhaus, M.S. Optical Properties of Carbon Nanotubes. In *Carbon Nanotubes and Graphene*; Elsevier: Amsterdam, The Netherlands, 2014; Volume 2014, pp. 77–98. ISBN 9780080982328. [CrossRef]

14. Pacheco, M.; Barticevic, Z.; Latge, A.; Rocha, C.G. Optical properties of carbon nanotubes under external electric fields. *Braz. J. Phys.* **2006**, *36*, 440–442. [CrossRef]

15. Blancon, J.-C. Optical absorption and electronic properties of individual carbon nanotubes. Ph.D. Thesis, Université Claude Bernard—Lyon I, Villeurbanne, France, 2013.

16. Chen, R.B.; Shyu, F.L.; Chang, C.P.; Lin, M.F. Optical Properties of Boron Nitride Nanotubes. *J. Phys. Soc. Jpn.* **2002**, *17*, 2286–2289. [CrossRef]

17. Wirtz, L.; Rubio, A. Optical and Vibrational Properties of Boron Nitride Nanotubes. *Irorun* **2009**, *13*, 105–148. [CrossRef]

18. Li, F.; Lu, J.; Tan, G.; Ma, M.; Wang, X.; Zhu, H. Boron nitride nanotubes composed of four- and eight-membered rings. *Phys. Lett. A* **2019**, *383*, 76–82. [CrossRef]

19. Kweitsu, E.O.; Armoo, S.K.; Kan-Dapaah, K.; Abavare, E.K.K.; Dodoo-Arhin, D.; Yaya, A. Comparative Study of Phosgene Gas Sensing Using Carbon and Boron Nitride Nanomaterials—A DFT Approach. *Molecules* **2020**, *26*, 120. [CrossRef]

20. Tang, Y.; Lu, J.; Liu, D.; Yan, X.; Yao, C.; Zhu, H. Structural Derivative and Electronic Property of Armchair Carbon Nanotubes from Carbon Clusters. *J. Nanomater.* **2017**, *2017*, 1–11. [CrossRef]

21. Piazza, V.; Gemmi, M. *Optical properties of boron nitride nanotubes: Potential exploitation in nanomedicine*; William Andrew Publishing: Norwich, NY, USA, 2016; pp. 139–147. [CrossRef]

22. Xu, Z.; Zhang, W.; Zhu, Z.; Ren, C.; Li, Y.; Huai, P. Effects of tube diameter and chirality on the stability of single-walled carbon nanotubes under ion irradiation. *J. Appl. Phys.* **2009**, *106*, 43501. [CrossRef]

23. Jafarzadeh, N.; Nadafan, M.; Malekfar, R.; Shakeri-Zadeh, A.; Meidanchi, A.; Eynali, S. Structural, optical and dielectric studies of Ag nanoparticles decorated by herceptin. *Phys. E Low-dimensional Syst. Nanostructures* **2019**, *114*, 113562. [CrossRef]

24. Nicolás, G.; Dorantes-Dávila, J.; Pastor, G. Calculation of orbital polarization effects in small Co clusters. *Comput. Mater. Sci.* **2005**, *35*, 292–296. [CrossRef]

25. Guo, X.; Yu, D.; Wu, J.; Min, C.; Guo, R. Effects of nanotube modification on the dielectric behaviors and mechanical properties of multiwall carbon nanotubes/epoxy composites. *Polym. Eng. Sci.* **2012**, *53*, 370–377. [CrossRef]

26. Slepchenkov, M.M.; Shmygin, D.S.; Zhang, G.; Glukhova, O.E. Controlling anisotropic electrical conductivity in porous graphene-nanotube thin films. *Carbon* **2020**, *165*, 139–149. [CrossRef]

27. Beni, Y.T.; Mehralian, F.; Zeverdejani, M.K. Free vibration of anisotropic single-walled carbon nanotube based on couple stress theory for different chirality. *J. Low Freq. Noise Vib. Act. Control* **2017**, *36*, 277–293. [CrossRef]

28. Wang, H.; Tam, F.; Grady, N.K.; Halas, N.J. Cu Nanoshells: Effects of Interband Transitions on the Nanoparticle Plasmon Resonance. *J. Phys. Chem. B* **2005**, *109*, 18218–18222. [CrossRef]

29. Zhan, Y.; Lago, E.; Santillo, C.; Castillo, A.E.E.D.R.; Hao, S.; Buonocore, G.G.; Chen, Z.; Xia, H.; Lavorgna, M.; Bonaccorso, F. An anisotropic layer-by-layer carbon nanotube/boron nitride/rubber composite and its application in electromagnetic shielding. *Nanoscale* **2020**, *12*, 7782–7791. [CrossRef]

30. Chen, H.; Chen, Y.; Liu, Y.; Xu, C.-N.; Williams, J.S. Optical properties of BN nanotubes. In Proceedings of the 2006 International Conference on Nanoscience and Nanotechnology, Brisbane, Australia, 3–7 July 2006. [CrossRef]

31. Gharbavi, K.; Badehian, H. Optical properties of armchair (7, 7) single walled carbon nanotubes. *AIP Adv.* **2015**, *5*, 77155. [CrossRef]

32. Toudert, J.; Serna, R. Interband transitions in semi-metals, semiconductors, and topological insulators: A new driving force for plasmonics and nanophotonics [Invited]. *Opt. Mater. Express* **2017**, *7*, 2299–2325. [CrossRef]

33. Radzwan, A.; Lawal, A.; Shaari, A.; Chiromawa, I.M.; Ahams, S.T.; Ahmed, R. First-principles calculations of structural, electronic, and optical properties for Ni-doped Sb2S3. *Comput. Condens. Matter* **2020**, *24*, e00477. [CrossRef]

34. Bolotin, D.S.; Novikov, A.S.; Kolesnikov, I.E.; Suslonov, V.V.; Novozhilov, Y.; Ronzhina, O.; Dorogov, M.; Krasavin, M.; Kukushkin, V.Y. Phosphorescent Platinum(II) Complexes Featuring Chelated Acetoxime Pyrazoles: Synthetic, Structural, and Photophysical Study. *ChemistrySelect* **2016**, *1*, 456–461. [CrossRef]

35. Tan, Y.C. Chemical Sensing Applications of Carbon Nanotube-Deposited Optical Fibre Sensors. *Chemosensors* **2018**, *6*, 55. [CrossRef]

36. Fahad, J.; Bhardwaj, A.K. Preparing Carbon Nanotubes (Cnts) for Optical System Applications. *Int. J. Nanotechnol. Appl.* **2013**, *2*, 21–38.

37. Jiang, L.; Liu, P.; Liu, C.; Fan, S. Enhanced light transmission of carbon nanotube film by ultrathin oxide coatings. *AIP Adv.* **2020**, *10*, 75304. [CrossRef]